Journal of Bio- and Tribo-Corrosion (2021) 7:59
https://doi.org/10.1007/s40735-021-00491-x

Tribocorrosion Behaviour of Biomedical Porous Ti–20Nb–5Ag Alloy in Simulated Body Fluid

M. J. Shivaram[1] · Shashi Bhushan Arya[1] · Jagannath Nayak[1] · Bharat B. Panigrahi[2]

Received: 4 September 2020 / Revised: 14 December 2020 / Accepted: 11 February 2021 / Published online: 5 March 2021

Abstract
Porous Ti–20Nb–5Ag (wt.%) alloy was developed using powder metallurgy (PM) route with the porosity of 43% after sintering in a high vacuum atmosphere. The microstructure of the porous alloy revealed various micro, macro and interconnected pores with an average pore size of about 114 µm. Tribocorrosion behaviour of the porous alloy was examined in simulated body fluid under the various applied load of 1–10 N using DC electrochemical corrosion technique and kinetic parameters (corrosion potential, corrosion current density and breakdown potentials). After tribocorrosion test, the OCP values decreased from 0.17 to − 0.49 V_{SCE} as applied load was increased. The potentiodynamic polarization results revealed that the corrosion potential decreased, while corrosion current density increased under higher applied loads. Active–passive transition plots showed metastable passivity due to severe fluctuations of passive current density. After tribocorrosion, the surface morphology was analysed using SEM, and it exhibited the severity of wear tracks at higher applied loads. The results indicated that the developed porous Ti–20Nb–5Ag alloys exhibit better tribocorrosion properties in simulated body fluid. Through observations of SEM images of the worn surfaces, the visible scratches and deep grooves were observed along the sliding direction, indicating a predominant abrasive mechanism.

Keywords Porous metal · Powder metallurgy · Tribocorrosion behaviour · Microstructure

1 Introduction

Recently, porous Ti alloys a gained significant interest in clinical applications, owing to their low elastic modulus, good corrosion resistance and excellent biocompatibility [1–3]. The introduction of pore structure decreases the mechanical properties of the implant materials. However, these pore structure provides most exciting property i.e. low elastic modulus which can significantly reduce the stress-shielding effect as compared to the bulk Ti alloy [4]. However, the pore structures not only help to minimize the stress-shielding effect but also increase new tissue ingrowth and transportation of body fluids. It is also noticed that the average pore size of more than 100 µm is more beneficial for facilitating a new bone ingrowth [5].

When the porous implants are attached to the human body, an initiation and growth of the new bone tissues on the surface enhances the osseointegration properties. Metallic passivity of alloy depends on alloying elements which significantly influence the surface properties of the implant materials such as new tissue in growth and corrosion behaviour [6–8]. The Ti–6Al–4V alloy is the most commonly used material for biomedical applications over the other metallic alloy such as austenitic stainless steels Co–Cr–Mo alloy [9, 10]. However, releasing of toxic metal ions (Al and V ions) from the alloy surface leads to the decrease in osseointegration and corrosion properties. The corrosion and antibacterial phenomenon due to the dissolution of Ti and its alloys are major concerns because of toxic ion release from the alloy surface [11].

Recently, new $\alpha+\beta$-type and β-type Ti-based porous alloys have been fabricated using various alloying elements such as Nb, Mo, Zr, Sn, Ta and Ag [12, 13]. However, Nb is identified as one of the major alloying element with the titanium which acts as a β stabilizer and explicitly reduces

✉ Shashi Bhushan Arya
sbarya@nitk.edu.in

[1] Department of Metallurgical and Materials Engineering, National Institute of Technology Karnataka, Surathkal, Mangaluru 575025, India

[2] Department of Materials Science and Metallurgical Engineering, Indian Institute of Technology Hyderabad, Kandi, Sangareddy, Telangana 502285, India

the elastic modulus of Ti-based alloy [14]. It is well reported that the Nb is a strong β stabilizer and good alloying element with Ti. Addition of Nb content in Ti alloys leads to the formation of $\alpha+\beta$ type, near β type and β type Ti alloys which is more beneficial to obtain lower elastic modulus, good corrosion resistance. Also, Nb has non-toxic and non-allergic properties to ensure stability in the human body without any adverse reaction with the surrounding tissues [15–17]. The addition of silver (Ag) in Ti matrix is an appropriate choice due to the potent antibacterial properties and the best result is reported up to 5% of Ag content to disrupt the bacterial growth on the implant surface [18].

Processing of porous Ti alloy using a PM technique offers the ability to control the pore morphology (pore size and shape) with good pore uniformity and interconnectivity. However, few limitations of using this processing technique, initiating from irregular and inhomogeneous distribution of pore structure by mixing the space holder and metal powder, were generated by irregular-shaped space holder particles and different sizes in elemental powders. Moreover, sintering process of Ti-based alloy is very difficult at high temperature because it is highly reactive and high affinity towards oxygen, which leads to form oxides. To avoid oxidation, the sintering process should be carried out in the control atmosphere (i.e. vacuum or argon atmosphere) to get sound and oxides free sintered products [19, 20].

However, knee and total hip joints experience a sliding contact during the motion of human body, constituting a tribocorrosion behaviour. Tribocorrosion is an irreversible degradation phenomenon due to the synergy of mechanical (wear) and environmental effects (corrosion), which could cause larger material damage than expected independently [21–23]. It involves numerous interaction effects between mechanical and electrochemical phenomena for the implant materials. An implant material inserted into human body undergoes continuous micro-movement, leading to material deterioration and release of wear debris into the body which significantly minimize the life span of the implants [24].

Ti-based alloy exhibits poor wear resistance which can damage the passive film in the corrosive environment. However, wear resistance of the passive film is easily removed as wear debris under the loading condition which has harmful effects on the surroundings of the bones [21, 25]. The simultaneous action of corrosion and wear releases the metallic ions, which can adversely affect the biocompatibility and mechanical integrity of implants. Therefore, the assessment of biomaterial to understand corrosion behaviour and corrosive wear is required to ensure the safety of implants in the body fluids of the human body.

Many researchers studied the tribocorrosion behaviour of the bulk Ti-based alloys in various body fluids [25–27]. However, Toptan et al. [28] have studied the tribocorrosion behaviour of porous titanium with a different porosity level of 22 and 37% in NaCl solution. They found a sudden decrease in OCP values due to the mechanical damage of passive film under the sliding conditions. There is limited literature available on the tribological properties concerning porous Ti-based alloy. In the present article, a novel porous Ti–20Nb–5Ag alloy is developed through the PM method using space holder materials. The microstructure and the tribocorrosion behaviour were investigated in the SBF under applied loads of 1, 5 and 10 N using electrochemical techniques. According to literature and the best of our knowledge, no tribocorrosion study has been performed on porous Ti–20Nb–5Ag alloy.

2 Experimental Details

2.1 Preparation of Porous Alloy

Commercially available pure elemental powders of Ti (~45 µm, purity of 99.5%), Nb (~45 µm, purity of 99.8%) and Ag (~5 µm, purity of 99.9%) were used to develop the porous Ti–20Nb–5Ag alloy using the PM method. The elemental powder with the nominal composition of Ti–20Nb–5Ag (wt.%) was ball milled for 20 h using a high-energy planetary ball mill (Retsch–PM100, Germany). A ball-to-powder ratio of 10:1 and rotation speed of 250 rpm were maintained. The ball-milled powder mixed with 30 wt.% of NH_4HCO_3 is used as a space holder material to achieve the required porosity. Blended powders were made compact at an applied load of 500 MPa to prepare a pellet with the dimensions ∅10 mm and 15 mm. The cylindrical compacts were heated at 200 °C for 2 h to eliminate space holder particles and sintered at 1200 °C for 3 h in a high vacuum furnace at a vacuum level of 10^{-5} mbar. The heating and cooling rates of 10 °C/min were maintained during the sintering process.

2.2 Tribocorrosion Performance in SBF Solution

Prior to tribocorrosion test, porous samples were polished with up to 1200 grit paper. The test was performed using a custom-made pin-on-disc tribometer [29]. The schematic representation of customized pin-on-disc type tribometer which was connected to a potentiostat is shown in Fig. 1. The three-electrode system is used to conduct the corrosion and tribocorrosion tests. The porous alloy was used as a working electrode, saturated calomel (SCE) as a reference electrode and platinum as a counter electrode. Alumina disc (∅10 mm and 5 mm thickness) was used as a counter surface with a roughness of 0.02 µm (according to the manufacturer). Various loads of 1, 5 and 10 N were applied to measure the tribocorrosion characteristics of porous alloys under the sliding velocity of 2 rpm. Simulated body fluid (SBF)

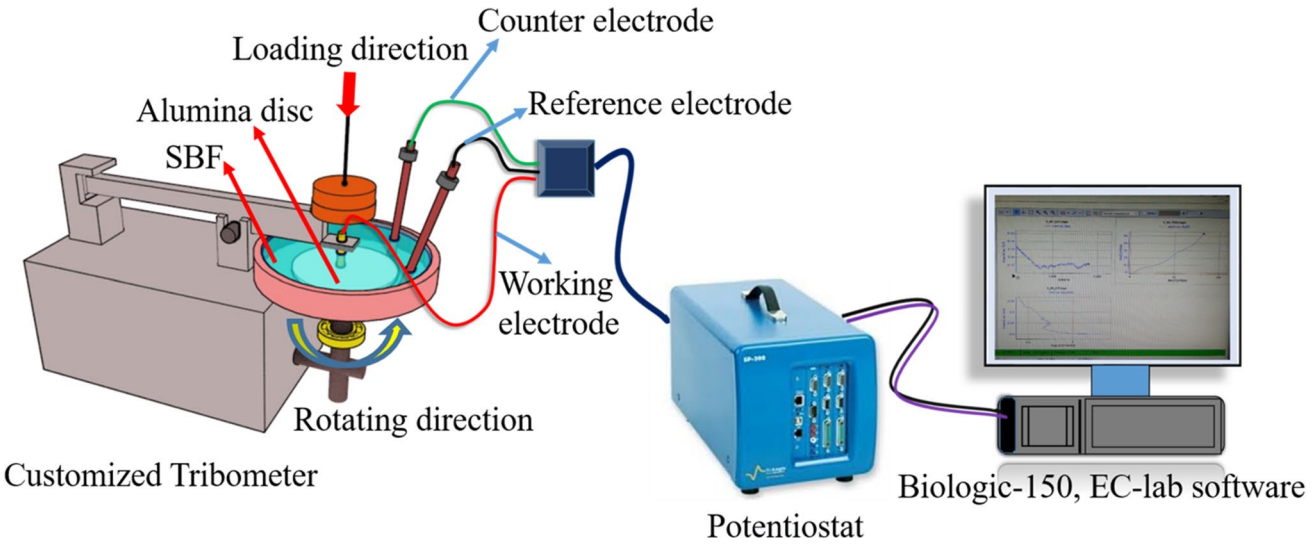

Fig. 1 Schematic representation of pin-on-disc type tribometer

was used as an electrolyte with a pH of 7.4 to conduct the tribocorrosion test [30]. Before conducting the tests, the porous alloys were kept for 30 min in the SBF for stabilization. Electrochemical techniques such as open-circuit potential (OCP) and potentiodynamic polarization (Biologic-potentiostat, SP–150, France) were used to examine tribocorrosion properties. Three specimens were performed for each loading condition in the tribocorrosion tests. The microstructure of the porous alloy was analysed using scanning electron microscopy (SEM, JEOL, JSM-6380LA, Japan).

2.3 Characterization of Developed Porous Alloys

The porosity and density of all the developed porous Ti–20Nb–5Ag alloys were measured by using Archimedes' immersion technique. Pore size of the sintered porous alloys was determined using the Image-J software and more than 100 pores were measured to determine the mean pore size. The following equations were used to measure the porosity and density.

$$\text{Porosity } (\%) = \frac{W_{sat} - W_{dry}}{W_{sat} - W_{sus}} \quad (1)$$

$$\text{Density} = \frac{W_{dry}}{W_{sat} - W_{sus}} \ (\text{g/cm}^3) \quad (2)$$

where W_{sat} is the saturate weight, W_{sus} is the suspended weight and W_{dry} is the dry weight.

The microstructures of the prepared Ti–20Nb–5Ag alloys before and after tribocorrosion tests were examined in a scanning electron microscope (SEM, JEOL, JSM–638OLA).

3 Results and Discussion

3.1 Microstructure of Porous Alloy

Figure 2a shows the SEM images of the porous Ti–20Nb–5Ag alloy which exhibit the porosity of about 43%. The microstructure of porous alloy exhibits the pores with an irregular shape and rough surface due to the evaporation of the used space holder particles. SEM image also shows the various forms of pores such as micros, macro and interconnected pores throughout the surface which facilitate to promote cell adhesion and bone ingrowth [1, 4]. The average pore sizes and pore distribution of developed porous alloys were measured using image-J software based on the SEM images. A pore size of more than 100 µm is more beneficial for facilitating a new bone ingrowth. When the porous implants are attached to the bone tissue, the initiation and growth of the new bone tissues on the porous surface enhance the osseointegration properties of implants [7, 15]. Figure 2b shows the distribution of pore size. It is found that the pore size is quite large as 400 µm with the average pore size about 114 µm which may be favourable for enhancing the osseointegration properties [12].

3.2 Tribocorrosion Test

The evaluation of OCP under applied loads (1, 5 and 10 N) in SBF for 900 s is shown in Fig. 3. Without loading condition, the OCP value observed is about 0.16 V_{SCE} and it shows the stable potential due to the formation of the spontaneous passive film on the sample. On the other hand, the OCP values were recorded as a function of time under the loading conditions which can be distinguished into three

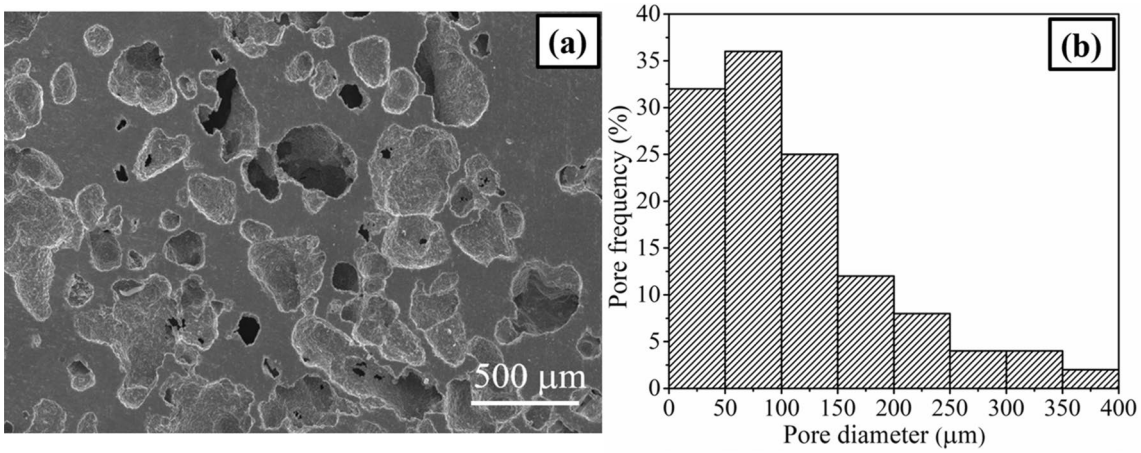

Fig. 2 **a** SEM images of porous Ti–20Nb–5Ag alloy and **b** pore size distribution

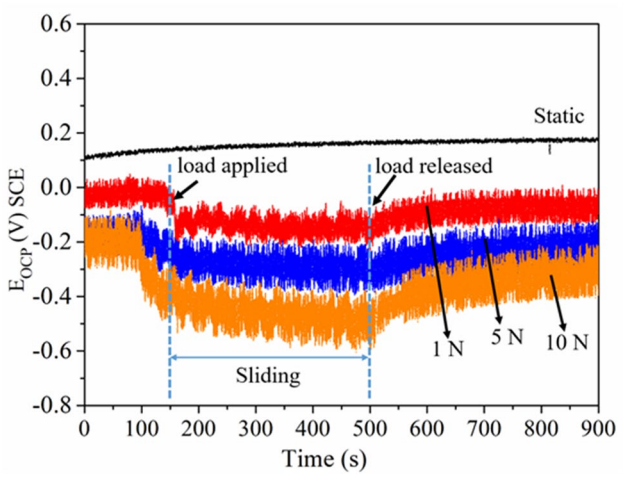

Fig. 3 Open-circuit potential (OCP) scan at static and various applied loading conditions

parts mainly before sliding (0 to 150 s), during sliding (150–500 s) and after sliding (500–900 s). It is noticed that the OCP values of all the porous samples were almost stable before applying a load. This is due to the formation of stable passivation film on the porous alloy surface. The potential values obtained were -0.14 V_{SCE}, -0.32 V_{SCE} and -0.49 V_{SCE} for the applied loads of 1, 5 and 10 N, respectively. The results indicate that the applied loads significantly effect the OCP of the porous alloy which are shifted towards a negative direction over the without loading condition. During the sliding process, the higher frictional forces are induced on increasing the application of applied load which can be difficult in the relative movement between the interfaces. This can be attributed to the destruction and delamination of passive film under the sliding process. However, there is a possibility of high material removal from the surface because of pore structures under the various applied loads [24, 28, 31]. It is also observed that there are more fluctuations in OCP due to the regeneration of new active surfaces when the material is removed under the applied load. Further, it is detected that the OCP values obtained during sliding are mixed potential values, which reflect both the active (worn) and passive (unworn) surfaces of the porous alloy [28].

Electrochemical polarization plots for porous Ti–20Nb–5Ag alloy were obtained without loading condition and under the influences of applied loads of 1–10 N in SBF solution and sliding against the counter surface (alumina disc) are shown in Fig. 4. The potentiodynamic polarization curves of the porous alloy without applying a load are shown in Fig. 4a. The porous alloy exhibits a typical active–passive transition behaviour with a stable passivation across the potential regions with lower passive current density indicating spontaneous passive film formation and its stability even at higher potentials. Potentiodynamic polarization curves measured under the applied loads of 1, 5 and 10 N are shown in Fig. 4b–d, respectively. The results show that there are no significant changes in the active–passive transition plots of the porous alloys. However, potentials shift in active direction is noticed on increasing the applied loads. The shift of corrosion potential is due to the higher frictional forces at the interface between porous alloy and harder counter surface which directly affect the spontaneous passive film [24]. Interestingly, it is observed that there are current fluctuations in the polarization curves under the applied loads. These fluctuations of currents densities were started near active area (-0.25 to $+0.25$ V_{SCE}) at lower weight of loading of 1 and 5 N (Fig. 4b, c) indicating initial dissolutions of metal due to higher electrochemical corrosion reaction rates. This result is mainly attributed to the rubbing action of porous alloy by counter surface which lead to the removal of the protective passive film of metallic oxides in the form of abrasion wear. However, it is not seen for the sample without loading (Fig. 4a) due to the absence

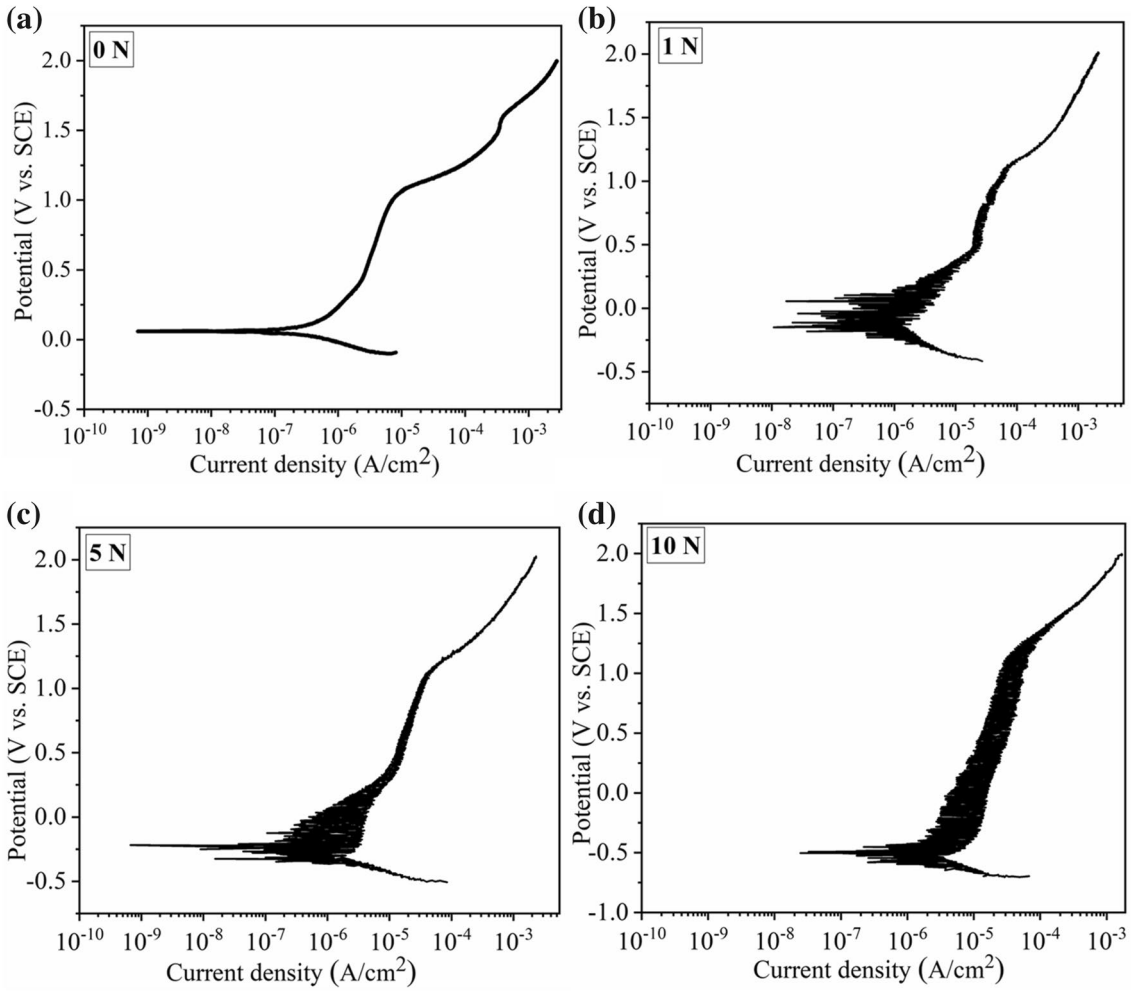

Fig. 4 Potentiodynamic polarization curves of porous Ti–20Nb–5Ag alloy at various applied loads: **a** 0 N, **b** 1 N, **c** 5 N and **d** 10 N

of rubbing action (without wear control) and well covered by a thin protective passive film in SBF solution. Further, at the applied load of 10 N (Fig. 4d), it is noticed that the current fluctuation is more and constant up to the higher potential range over the 1 and 5 N. Results indicate that more oscillations were observed on the current density values because of repeated action of depassivation and repassivation on the alloy surface. This is due to the frictional force that occurs between the interfaces [32]. As the wear action removes the passive layer from the porous alloy surface on local anodic region, passivation occurs simultaneously. However, it was observed that the rapid passivation and removal of passive film result in high current fluctuations at lower anodic potentials [32, 33].

For better understanding of the polarization behaviour of the porous Ti–20Nb–5Ag alloy with/without loading, the corrosion parameters such as corrosion potential (E_{corr}) and current density (i_{corr}) are measured by analysing the Tafel region through anodic (β_a) and cathodic (β_c) branches and the results are presented in Table 1. It can be seen that there

Table 1 Corrosion parameters of porous alloy in SBF solution

Load (*N*)	E_{corr} (V_{SCE})	β_a (*V*/dec)	β_c (*V*/dec)	i_{corr} (μA/cm^2)	i_{pass} (at 0.5 V) (μA/cm^2)	Corrosion rate (mpy) × 10^{-3}
Static	0.06 ± 0.02	0.18 ± 0.07	0.09 ± 0.02	0.17 ± 0.05	0.003 ± 0.04	7.14 ± 0.30
1	− 0.17 ± 0.03	0.28 ± 0.04	0.11 ± 0.02	0.20 ± 0.04	0.013 ± 0.02	8.40 ± 0.9
5	− 0.22 ± 0.04	0.39 ± 0.03	0.13 ± 0.05	0.33 ± 0.10	0.014 ± 0.04	13.8 ± 0.51
10	− 0.49 ± 0.04	0.28 ± 0.05	0.14 ± 0.04	0.48 ± 0.1	0.020 ± 0.05	20.17 ± 0.83

is a remarkable shift towards the negative direction of the corrosion potential from the 0.06 V_{SCE} to −0.49 V_{SCE}, with a slight increase in the corrosion current density from 0.17 to 0.48 μA/cm^2. This indicates the decrease in corrosion resistance with the increase in the applied loads.

Figure 5 shows the SEM micrographs of Ti–20Nb–5Ag porous alloy after the tribocorrosion test. The abrasion was the main mechanism under sliding at various applied loads (1, 5 and 10 N). An increase in narrow ploughing is observed which is caused by applied loads and relative sliding movement between the interfaces. At 10 N load, more narrow wear tracks with deep grooves were observed compared to 1 and 5 N. However, the wear debris plays an important role in tribocorrosion which acts as third-body abrasive particles, resulting in the increase of wear under the applied loads. Moreover, the porous alloy having irregular and non-homogeneous surface area may lead to the increase in the more wear debris and wear tracks with applied load increased [28, 34].

3.3 Mechanism of Material Removal from Porous Alloy

The mechanism of tribocorrosion process of porous Ti–20Nb–5Ag alloy in SBF solution is shown in Fig. 6. The tribocorrosion process takes place at both the electrochemical corrosion and wear that occur in the electrolyte medium. In the present study, pin-on-disc type and SBF were used as electrolyte to conduct the tribocorrosion behaviour of the porous alloy. Figure 6a shows the without applied load (static) conducting the test on porous Ti–20Nb–5Ag in SBF solution. It is reported that Ti and its alloys have native passive film which helps to enhance corrosion resistance [21, 35]. In the present study, the high potential (OCP) value was obtained for without applied load because of the protective and compact passive film formation on the alloy surface as compared to the applied load condition (as seen in Fig. 3). On other hand, applying load from the top end made the porous alloy come into contact with the counter surface (Alumina disc) (Fig. 6b), which generates the frictional forces at the interfaces and subsequently damage of passive film formed on the alloy surface (Fig. 6c). However, at the applied of 1 N, it can be seen that very small wear debris were worn out from the surface due to the damage of passive film by friction as seen in Fig. 6d. When applying a slightly higher load (5 N), a trivial removal of debris from the surface could be seen as shown in Fig. 6e which is supporting through the electrochemical corrosion kinetics data as the passive current density did not increased at 5 N as compared to load of 1 N. Interestingly, Fig. 6f shows more wear particles removal from the surface at an applied load of 10 N as compared to 1 N and 5 N (very high corrosion rate as well as passive current density). This is due to the rupturing of protective passive films which continually deformed plastically at higher applied loads because of high frictional forces at 10 N (Fig. 6e).

Pore morphology also plays and contributes a major role for the removal particles due to corrosive-wear test which acts as a third body (abrasive particles) under the sliding condition. Therefore, the main wear mechanism of the

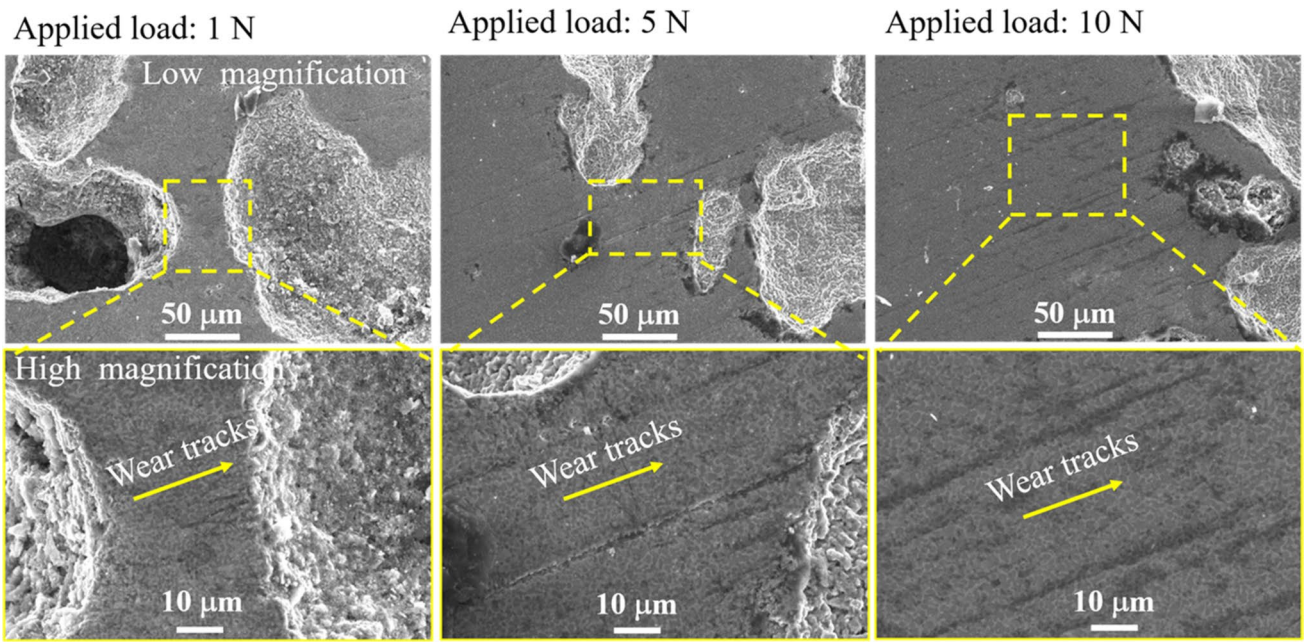

Fig. 5 SEM images of porous alloy after tribocorrosion at various applied loads

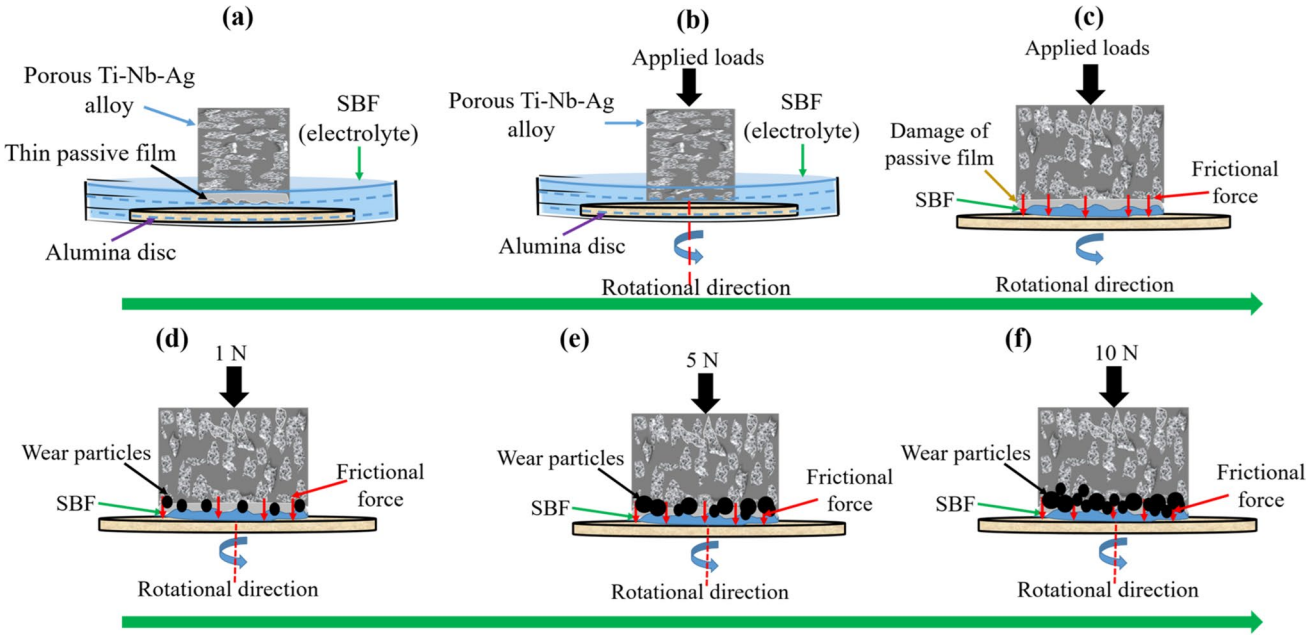

Fig. 6 Mechanism of tribocorrosion process of porous Ti–20Nb–5Ag alloy in SBF solution

tribocorrosion process is abrasive wear [28, 36]. During the tribocorrosion test, a thin passive film is removed from the surface as applied load increased and resulted in the formation of visible wear tracks on the alloy surface. However, the edges of the pore cells are quite sharp and it may easily break under the load, which leads to increase in the surface of pore area as well as excess wear debris. The accumulation of the wear debris into the surface of the pores might decrease the effect of the third body on the wear, and may also give rise to the damage of the passive film. However, the tear of pore cell wall edges is directly influenced on the increase of the pore area and slightly increases the groove formation under the applied load. In the present study, a thin passive film deforms plastically and the growing deepens grooves and roughens the surface of porous alloy. The rotational speed used in the present experiment is relatively small, and heat produced by rotation speed is negligible. However, both the action of loading and rotating cause the damage of passive film which is formed on the porous alloy surface. Moreover, the edges of these pore cells could be easily removed under the loads, which leads to the removal of wear debris from the porous alloy surface and significantly increases the wear tracks [24, 25, 28].

Huang et al. [35] investigated the wear–corrosion experiments Ti–25Nb–3Mo–3Zr–2Sn alloys in simulated physiological solutions under synergistic attacks of corrosion and wear. The result shows that the corrosion resistance of the alloy was decreased under the load as compared to static condition. It was found that the main tribological mechanisms were typically abrasive with adhesive wear. They formed passive film on the alloy wear-out as abrasive particles under the applied load. They also examined the chemical composition of passive film using XPS. It revealed that the passive films consist of TiO_2 and Nb_2O_5 are the major compounds in film, which is highly stable and able to protect against the corrosion attack. Similarly, other studies have reported that the chemical compositions of these oxide layers were responsible to enhance the corrosion resistance of Ti–Nb-based alloys and protects from the corrosion attack in simulated physiological solutions [37, 38].

Zhang et al. [39] have studied the effect of addition of various Ag content (7 and 10 at.%) on corrosion behaviour of Ti–Ag alloy in artificial body fluid. The result indicate that the addition of Ag to Ti is found to significantly minimize the corrosion current density and increase the open-circuit potential of Ti–Ag alloy. It also exhibited, a reduced passivation corrosion density with the addition of Ag content. The obtained result indicated that the addition of Ag attributed to the increase of corrosion resistance and it consists of two major reasons. Firstly, the formation of Ti_2Ag intermetallic precipitates which is confirmed by XRD analysis. Secondly, the surface samples which consisted of TiO_2 and Ag_2O oxides in a physiological solution, which is confirmed by XPS analysis. According to the previous studies on Ti-based alloys, the alloying elements play an important role on improving the corrosion resistance as they form various stable oxides on their surface. In the present study, porous Ti alloy developed with the addition of Nb and Ag alloying elements in Ti. As reported in the earlier studies, the possible formation of oxides on the porous alloy

surface such as TiO_2, Nb_2O_5 and Ag_2O in simulated body fluid contribute in enhancing the corrosion resistance of the porous alloys. Moreover, the XRD analysis of the developed porous Ti–20Nb–5Ag alloy exhibits the formation of Ti_2Ag intermetallic compound, which significantly enhances the corrosion resistance of the porous alloys in SBF [40]. The influence of intermetallic (as cathodic kinetics) and formation of oxides (Passivity) in SBF solution significantly influence the obtained results of static (without load) condition. However, by the synergic effect of corrosion and wear the stable oxides film mostly breakdown under the applied load, which gradually reduces the corrosion resistance of porous alloys.

4 Conclusions and Insight for Future

In summary, the porous Ti–20Nb–5Ag alloy with porosity of 43% was developed using the PM method. The microstructure consists of micropores, macropores and interconnected pores with the average pore size about 114 µm. After tribocorrosion, it was observed that there was a decrease in OCP from 0.17 to − 0.49 V_{SCE} with the increase in the applied loads. The potentiodynamic polarization results revealed that the corrosion potential shifted to the negative direction and corrosion current density increased. The results indicate that increasing the applied loads significantly increases the corrosion current density and corrosion rate due to the breakdown of passive film. However, further studies are necessary to understand the tribocorrosion behaviour of porous Ti–20Nb–5Ag alloy with respect to various porosity levels and applied loads, as well, fretting corrosion tests in order to simulate better bone/implant interface. Additionally, it is very much necessary to conduct in vitro, in vivo and antibacterial studies on this developed porous alloy to ensure the biocompatibility properties for bio-implant applications in the future.

Acknowledgements One of the authors, Mr. Shivaram M. J., would like to thank the Ministry of Human Resource Development (MHRD), Government of India for providing research fellowship. He would also like to thank Dr. Rahul B. Mane, (IIT Hyderabad) and Mr. Gurudath B. (NITK Surathkal) for their partial assistance in preparing the porous alloy samples. SB Arya another author would like to thanks Department of Science and Technolgy, Govt. of India.

References

1. Gao et al (2012) Mechanical modulation and bioactive surface modification of porous Ti–10Mo alloy for bone implants. Mater Des 42:13–20
2. Hsu HC et al (2015) Fabrication and characterization of novel porous titanium microspheres for biomedical applications. Mater Charact 106:317–323
3. Runa MJ et al (2013) Tribocorrosion response of the Ti6Al4V alloys commonly used in femoral stems. Tribiology Int 68:85–93
4. Torres-Sanchez C et al (2018) Porosity and pore size effect on the properties of sintered Ti35Nb4Sn alloy scaffolds and their suitability for tissue engineering applications. J Alloys Compd 731:189–199
5. Hsu HC et al (2010) Formation of calcium phosphates on low-modulus Ti–7.5Mo alloy by acid and alkali treatments. J Mater Sci 45:3661–3670
6. Spoerke ED et al (2005) A bioactive titanium foam scaffold for bone repair. Acta Biomater 1:523–533
7. Xiong J et al (2008) Mechanical properties and bioactive surface modification via alkali-heat treatment of a porous Ti–18Nb–4Sn alloy for biomedical applications. Acta Biomater 4:1963–1968
8. Mathew MT et al (2010) Tribocorrosion behaviour of TiC_xO_y thin films in bio-fluids. Electrochim Acta 56:929–937
9. De Assis SL et al (2006) Corrosion characterization of titanium alloys by electrochemical techniques. Electrochim Acta 51:1815–1819
10. Mathew MT et al (2011) Tribocorrosion behavior of CoCrMo alloy for hip prosthesis as a function of loads: a comparison between two testing systems. Wear 271:1210–1219
11. Fatehi K et al (2008) In vitro biomimetic deposition of apatite on alkaline and heat treated Ti6Al4V alloy surface. Bull Mater Sci 31:101–108
12. Aguilar C et al (2016) Synthesis and characterization of Ti–Ta–Nb–Mn foams. Mater Sci Eng C 58:420–431
13. Stráský J et al (2017) Increasing strength of a biomedical Ti–Nb–Ta–Zr alloy by alloying with Fe, Si and O. J Mech Behav Biomed Mater 71:329–336
14. Liu Q et al (2013) α′ type Ti–Nb–Zr alloys with ultra-low Young's modulus and high strength. Prog Nat Sci Mater Int 23:562–565
15. Rao X et al (2014) Phase composition, microstructure, and mechanical properties of porous Ti–Nb–Zr alloys prepared by a two-step foaming powder metallurgy method. J Mech Behav Biomed Mater 34:27–36
16. Nazari KA et al (2015) Mechanical properties and microstructure of powder metallurgy Ti–xNb–yMo alloys for implant materials. JMADE 88:1164–1174
17. Lee CM et al (2002) Structure–property relationship of cast Ti–Nb alloys. J Oral Rehabil 29:314–322
18. Hou L et al (2013) Fabrication and characterization of porous sintered Ti–Ag compacts for biomedical application purpose. J Mater Sci Technol 29:330–338
19. Lee B et al (2014) Space-holder effect on designing pore structure and determining mechanical properties in porous titanium. Mater Des 57:712–718
20. Shivaram MJ et al (2020) Electrochemical corrosion and impedance studies of porous Ti–xNb–Ag alloy in physiological solution. Trans Indian Inst Met 73:921–928
21. Pina VG et al (2016) Microstructural, electrochemical and tribo-electrochemical characterisation of titanium–copper biomedical alloys. Corros Sci 109:115–125
22. Mathew MT et al (2009) Significance of tribocorrosion in biomedical applications: overview and current status. Adv Tribol. https://doi.org/10.1155/2009/250986
23. Stack MM et al (2011) Tribology international some views on the construction of bio-tribo-corrosion maps for titanium alloys in Hank's solution: particle concentration and applied loads effects. Tribiol Int 44:1827–1837
24. Wang Z et al (2018) Tribocorrosion behavior of Ti–30Zr alloy for dental implants. Mater Lett 218:190–192

25. Diomidis N et al (2012) Tribo–electrochemical characterization of metallic biomaterials for total joint replacement. Acta Biomater 8:852–859
26. More NS et al (2011) Tribocorrosion behavior of β titanium alloys in physiological solutions containing synovial components. Mater Sci Eng C 31:400–408
27. Dimah MK et al (2012) Study of the biotribocorrosion behaviour of titanium biomedical alloys in simulated body fluids by electrochemical techniques. Wear 295:409–418
28. Toptan F et al (2017) Biomedical materials tribocorrosion behavior of bio-functionalized highly porous titanium. J Mech Behav Biomed Mater 69:144–152
29. Vats V et al (2018) Tribo-corrosion study of nickel-free, high nitrogen and high manganese austenitic stainless steel. Tribol Int 119:659–666
30. Tk Ã, Takadama H (2006) How useful is SBF in predicting in vivo bone bioactivity? Biomaterials 27:2907–2915
31. Wang Z et al (2017) Tribocorrosion behaviour of a biomedical Ti–25Nb–3Mo–3Zr–2Sn alloy in Ringer's solution. Mater Sci Eng C 76:1094–1102
32. Yenal S et al (2013) Tribocorrosion behavior of duplex treated pure titanium in simulated body fluid. Wear 302:1642–1648
33. Toptan F et al (2016) Corrosion and tribocorrosion behavior of Ti–B_4C composite intended for orthopaedic implants. J Mech Behav Biomed Mater 61:152–163
34. Toptan F et al (2019) Corrosion and tribocorrosion behaviour of Ti6Al4V produced by selective laser melting and hot pressing in comparison with the commercial alloy. J Mater Process Technol 266:239–245
35. Huang W et al (2015) Wear and electrochemical corrosion behavior of biomedical Ti–25Nb–3Mo–3Zr–2Sn alloy in simulated physiological solutions. J Bio Tribo Corros 1:1–10
36. Fellah M et al (2019) Preliminary investigation on the bio-tribocorrosion behavior of porous nanostructured β-type titanium based biomedical alloys. Mater Lett 257:126–129
37. Guo X et al (2017) Corrosion and electrochemical impedance properties of Ti alloys as orthopaedic trauma implant materials. Int J Electrochem Sci 12:9007–9016
38. Vishnu DSM et al (2018) Electrochemical synthesis of porous Ti–Nb alloys for biomedical applications. Mater Sci Eng C 96:466–478
39. Zhang BB et al (2008) Effect of Ag on the corrosion behavior of Ti–Ag alloys in artificial saliva solutions. Dent Mater 25:672–677
40. Shivaram MJ et al (2020) Development and characterization of biomedical porous Ti–20Nb–5Ag alloy: Microstructure, mechanical properties, surface bioactivity and cell viability studies. Metals Mater Inter. https://doi.org/10.1007/s12540-020-00915-2